
Volume 15, Issue 3, 152527 (1-10)

Iranian Journal of Catalysis (IJC)

https://doi.org/10.57647/j.ijc.2025.1503.27

# Production of $Ag_3PO_4$ from natural phosphate for visible-light photocatalytic degradation of oxytetracycline antibiotic

Sara Fatine[1], Jihane Labrag[1], Abdeladim Oulguidoum[1], Abdelaziz Laghzizil[1,*], Jean Michel Nunzi[2]

[1]*Laboratory of Applied Chemistry of Materials, Faculty of Science, Mohammed V University in Rabat, Avenue Ibn Batouta BP.1014, Rabat, Morocco.*
[2]*Department of Chemistry, Queen's University, Kingston, ON K7L 3N6, Canada.*

[*]**Corresponding author:** laghzizi@fsr.ac.ma

**Original Research**

Received:
4 February 2025
Revised:
8 May 2025
Accepted:
25 May 2025
Published online:
28 May 2025
Published in issue:
30 September 2025



**Abstract:**

Natural phosphate was valorized as a precursor for the synthesis of the highly efficient photocatalytic material silver phosphate ($Ag_3PO_4$). A straightforward synthesis method involving the dissolution of the natural phosphate followed by the precipitation of particles was optimized for the silver phosphate preparation. Physicochemical properties of the particles were characterized using various techniques. The photodegradation rate of oxytetracycline (OTC) antibiotic under visible light by the $Ag_3PO_4$ particles exceeded 86%, depending on the operating conditions. The effect of OTC concentration, pH of the solution, and catalyst calcination was studied to investigate the antibiotic degradation. Hole ($h^+$) reactive species were the main participants in OTC oxidation; meanwhile, $^{\bullet}O^{2-}$ and $OH^{\bullet}$ contributed to the degradation process. Improved performance can be attributed to the porous structure, which provides homogeneous active sites for antibiotic adsorption, followed by complete photodegradation. The nanocomposites were easily recycled at 500 °C without loss of catalytic efficiency. Therefore, porous $Ag_3PO_4$ catalyst is an effective and environmentally friendly means to remove various organic pollutants from water.

**Keywords:** Antibiotic residue; $Ag_3PO_4$; Natural phosphate; Photocatalytic degradation

## 1. Introduction

Water pollution is caused by the presence of microorganisms, chemical substances, and industrial waste [1, 2]. The major processes in conventional wastewater treatment plants are chemical coagulation, flocculation, sedimentation, filtration, and disinfection, but they have the disadvantage of not degrading the pollutants, which will concentrate in the solid phase, generating a new source of pollution. Several porous adsorbent/photocatalytic materials were applied to water treatment, in which coupled adsorption and photodegradation are promising methods to reduce or eliminate the risks of toxic organic species in water [3]. Pharmaceutical residues were considered a class of emerging pollutants due to their intensive use and persistence in the environment, even at low concentrations. Most of these are antibiotics, defined as chemical compounds with antibacterial properties. Antibiotics, which are released into the environment without any prior treatment, in the form of metabolites, by-products, and parent compounds, can contaminate water and soil. They are a potential risk for many organisms present in the environment. Photocatalysis appears to be a promising technology to remediate these issues by enabling the degradation of organic pollutants through the activation of semiconductors by light. When a semiconductor is irradiated by photons of energy equal to or greater than the energy gap ($E_g$) of this semiconductor, subjected to UV, visible or solar irradiation, electron and hole ($e^-/h^+$) pairs can be induced in the conduction band (CB) and the valence band (VB) of the semiconductor, respectively [4, 5]. $TiO_2$

and ZnO are the most studied thanks to their photocatalytic efficiency, but they are only active under UV irradiation, which constitutes only around 4% of the solar energy [6, 7]. Silver-based photocatalysts possess great significance for photocatalysis owing to their attractive properties under visible light, including $Ag_2O$, $Ag_2S$, AgX (X, Cl, F, I), and $Ag_3PO_4$ [8, 9]. The increased photoactivity is related to the presence of the metallic Ag nanoparticles that extend light response towards the visible light region, and to their better charge transfer ability. However, photo corrosion and photosensitization of these catalysts limit their regeneration after a few cycles. Plasmonic nanophotocatalysts powered by sunlight provide advanced photochemical conversion and photoreduction approaches [10]. To stabilize them and accelerate the recombination of photogenerated carriers, their combination with semiconductors and/or porous materials constitutes an effective approach to improve the overall photocatalytic efficiency [10, 11]. Silver phosphate $Ag_3PO_4$ is highly efficient at generating reactive species, and it promotes photocatalysis under visible light owing to its wide energy band gap, between $2.2 - 2.7$ eV depending on its mode of preparation [12–14]. The suitability of $Ag_3PO_4$ as a photocatalyst was evaluated for the degradation of several organic pollutants [15–17]. It exhibits excellent catalytic activity for the reduction of p-nitrophenol and $Cr^{4+}$ [18, 19], and it has antibacterial properties. Its photocatalytic efficiency depends on the synthesis conditions and on its structural and textural properties [20, 21]. The photocatalytic activity of porous $Ag_3PO_4$ can be tuned by different parameters [22]: Crystal structure, purity, particle shape and size, and their surface area [23–25]. Another important parameter for a photocatalyst is its manufacturing cost. $Ag_3PO_4$ photocatalysts were fabricated using many techniques, including precipitation, hydrothermal, sol-gel, sonochemistry, and thermal decomposition from commercial precursors [23–30]. The reaction efficiency and microstructure of the chemically obtained particles can be controlled and stabilized by changing the raw materials [31, 32]. Recently, a natural phosphate (NP) mineral was used as a raw material to prepare a novel and efficient hydroxyapatite by a dissolution and precipitation method [33]. This converted apatite material was developed as a novel adsorbent for the removal of organic and inorganic pollutants from aqueous environments [34, 35].

We tested the potential of this approach with a natural phosphate rock from Morocco to prepare porous $Ag_3PO_4$. Interestingly, Morocco has three-quarters of the world's phosphate reserves. The conversion of natural phosphate into silver phosphate was never reported or documented, though $Ag_3PO_4$ is an efficient photocatalyst for the degradation and mineralization of antibiotic residues in water. The structure and composition of the obtained material were characterized by different analytical techniques. Its catalytic efficiency was tested for the photodegradation under visible light of oxytetracycline (OTC) as an antibiotic model. This study highlights the effectiveness of $Ag_3PO_4$ as a photocatalyst as well as its potential to valorize natural phosphates into innovative and sustainable environmental applications.

## 2. Experimental

### 2.1 Preparation and characterization of the $Ag_3PO_4$ nanocomposites

The converted $Ag_3PO_4$ powder was prepared by dissolution/precipitation of a natural phosphate in the presence of $Ag^+$ ions. Natural phosphate was extracted from the Khouribga region of Morocco. As described in our previous hydroxyapatite synthesis work [33], 30 grams of the phosphate rock is first dissolved in 200 mL of aqueous solution containing 20 mL of nitric acid (65%) to get the $Ca^{2+}$ and $H_3PO_4$ at room temperature (24 °C). After separation of insoluble compounds such as residual clays by filtration, the filtrate was added dropwise to the second solution composed of silver nitrate and an optimized volume of concentrated ammonia (25%, Aldrich Co.) varying the alkaline pH from 8 to 12 (Fig. 1). After calculating the amount of phosphorus produced from 30 grams of NP dissolved in a total volume of 400 mL of distilled water, a sample of 12.8 mL of the filtrate (i.e. 4.766 mmol of phosphorus P) was added to the solution containing 14.399 moles of $Ag^+$ from $AgNO_3$ (form Aldrich Co.) and ammonia to obtain a theoretical Ag:P weight ratio equal to 3 necessary for production of stoichiometric silver phosphate called $Ag_3PO_4$. The mixture is


**Figure 1.** Protocol for $Ag_3PO_4$ synthesis from natural phosphate.

left stirring for 3 hours, then placed in an ultrasonicator in a water bath (35 kHz) for 30 min. Then, it is centrifuged at 4000 rpm for 15 min and dried at 100 °C overnight, before calcination at 300 °C and 500 °C for 3 hours. Under these conditions, specific particles were characterized by analytical techniques in order to study their structural, textural, and catalytic properties.

### 2.2 Photodegradation procedure

The photocatalytic efficiency of $Ag_3PO_4$ powders dried at 100 °C and calcined at 300 °C and 500 °C was evaluated under visible light (LED lamps in series with total power of 18 W) using a home-made 250 mL helical Pyrex photoreactor. The photoreactor was protected to minimize the transfer of light to the external environment. The source of irradiation was placed in the center of the reactor to ensure the maximum energy exchange between the irradiation source and the reaction mixture. 200 mg of powder was preliminary dispersed in 100 mL of a 5 to 20 mg/L antibiotic solution at pH 4 to 10, and left for 30 min stirring in the dark. The solution was then exposed to visible light under magnetic stirring. At different reaction times ($t$), aliquots of the supernatant solution were taken with a 2 mL propylene syringe equipped with a 0.45 $\mu$m filter. The residual concentration of OTC $q_t$ (mg/g) was determined by UV-visible spectroscopy at $\lambda_{max} = 375$ nm.

## 3. Results and discussions

### 3.1 Characterization of the natural phosphate

Characterization of the Moroccan natural phosphate from the Khouribga region was carried out qualitatively and quantitatively. The rock phosphate was crushed and washed, and a particle size fraction of 100 to 400 $\mu$m was washed several times with distilled water to eliminate soluble materials, and then dried in an oven. Additional sieving makes it possible to refine the particle size to a range between 63 and 125 $\mu$m, thus yielding homogeneous grains adapted to optimal reactivity [36]. Figure 2 (a) shows the NP diffractogram, which is similar to well-crystallized fluorapatite (JCPDS #34-0011). In addition to the apatite phase, silica in the form of quartz ($SiO_2$) and calcite ($CaCO_3$) is identified. Infrared spectroscopy highlights the absorption bands of the $PO_4$ groups located between 1100 and 950 $cm^{-1}$ (symmetric and antisymmetric P-O vibration) and between 571 and 601 $cm^{-1}$ (O-P-O deformation) (figure 2 (b)). Other bands linked to the vibrations of the carbonates of NP, which is a carbonated fluorapatite of formula Ca10-xNax(PO4)6-x(CO3)xF2, are detected at 1458, 1430, and 871 $cm^{-1}$ [37]. This is also confirmed by the following chemical analyzes by X-ray fluorescence: Ca (37.84%), P (15.03%), F (2.84%), Si (1.78%), S (0.78%), Na (0.79%) plus other negligible elements containing small amounts of organic compounds for 7% by weight. The Ca/P molar ratio is 1.84, a value slightly higher than that of a stoichiometric FAP (Ca/P = 1.667) [37]. This variation is linked to the presence of carbonates in the NP mineral, which replace the phosphate groups as described previously [33]. The characterization of the selected natural phosphate NP reveals that it must be a good precursor of phosphorus to produce the silver phosphate $Ag_3PO_4$. According to the solubility constants of calcium and silver phosphates [19], $PO_4^{3-}$ has more affinity towards $Ag^+$ ions than $Ca^{2+}$ ions; the latter, which have not reacted, will be found in the filtrate after precipitation of the yellow $Ag_3PO_4$.

### 3.2 Characterization of the converted $Ag_3PO_4$ material

Figure 3 shows the X-ray pattern of $Ag_3PO_4$ samples synthesized at different pH and dried at 100 °C. At pH 8 and 10, the diffraction peaks of $Ag_3PO_4$ are sharp, intense, and well defined, reflecting the high crystallinity of the synthesized material. They are typical of those of standard $Ag_3PO_4$ synthesized from commercial precursors (called REF in Fig. 3) and correspond well to the reference pattern listed in ICDD PDF No. 06-0505. The converted $Ag_3PO_4$ dried at 100 °C crystallizes in the cubic system with the space group P-43n. Its cubic lattice parameter was calculated from X-ray diffraction(XRD) data using Bagg's law based

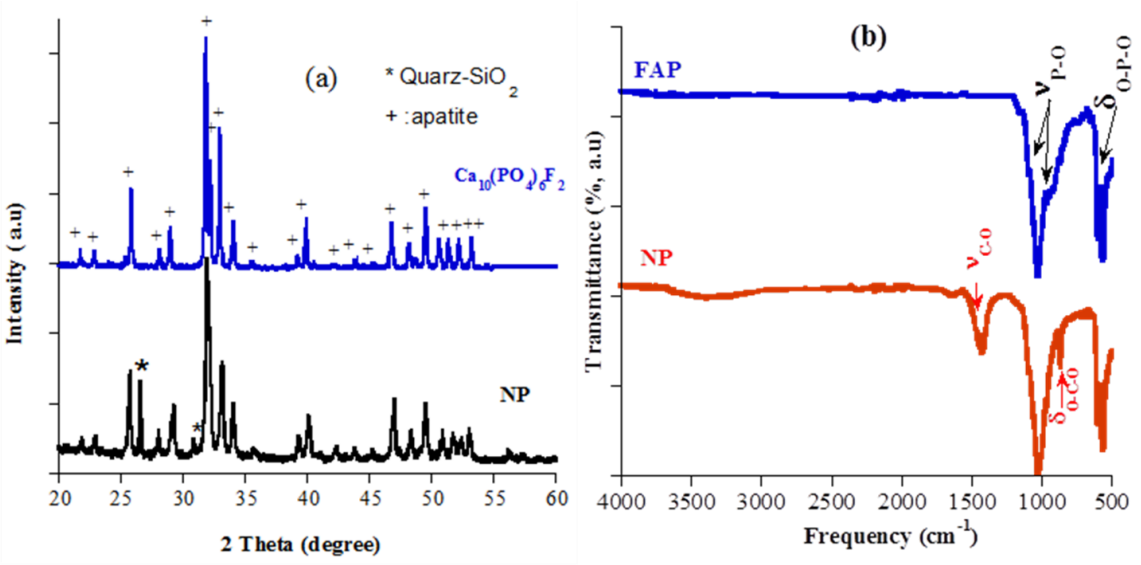


**Figure 2.** (a) XRD patterns, (b) FT-IR spectra of NP compared to synthetic FAP.

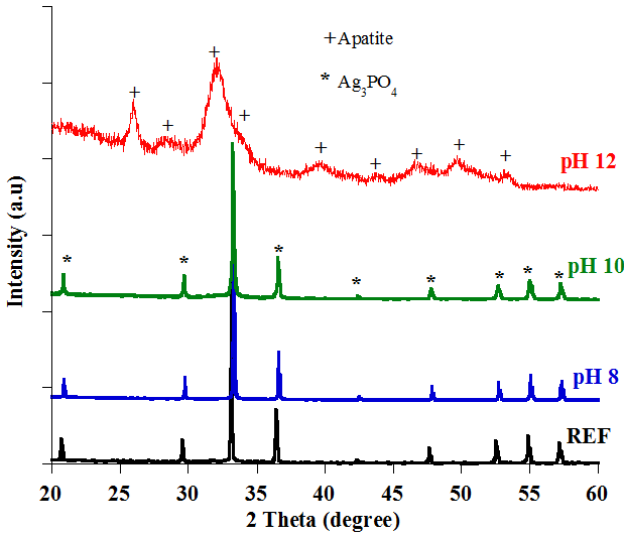


**Figure 3.** XRD patterns of $Ag_3PO_4$ prepared at various pH levels of the solution. REF sample is designated $Ag_3PO_4$ synthesized using commercial precursors [31].

on the following equation: $a = d\sqrt{+h^2+k^2+l^2}$; where $d$ is the interplanar spacing derived from the $2\theta$ values of the diffraction peaks, and $(hkl)$ are the Miller indices of the corresponding crystal planes. The lattice parameter is $a = (6.012 \pm 0.003)$ Å. No peaks for other phases, such as calcium phosphate, are detected, indicating that the $Ag^+$ ions have a good chemical affinity towards the $PO_4^{3-}$ anions, unlike the $Ca^{2+}$ ions coming from raw NP, which remained in the solution in their unreacted ionic form and were separated from the solid by washing. On the other hand, a poorly crystalline apatite structure appears at pH 12, demonstrating that pH variation influences the structural development of $Ag_3PO_4$ from the natural phosphate. At this pH value, it is in fact very likely that the $Ag^+$ ions were precipitated with the $OH^-$ ions or complexed with ammonia in the form of amorphous phases, while the $Ca^{2+}$ ions interact with $PO_4^{3-}$ to form apatite, which is consistent with our previous studies [7, 33].

The size of the crystallites $D$ in $Ag_3PO_4$ was estimated from the Debye-Scherrer equation [38]: $D = K\lambda/\beta\cos\theta$, where $K$ represents the Scherer constant (0.98), $\lambda$ denotes the wavelength (1.5406 Å), $\beta$ denotes the full width at half maximum (FWHM) of the peak in radians corrected for instrumental broadening. For $Ag_3PO_4$ powder dried at 100 °C, $D$ is 24 nm, while that calcined at 500 °C, it is 41 nm. Heat treatment of the $Ag_3PO_4$ powder synthesized at pH 8 (figure 4) at 300 °C and 500 °C results in a stable cubic crystal structure. The lattice parameter shows only a slight variation with temperature, reaching a value of $a = (5.992 \pm 0.004)$ Å at 500 °C. With increasing temperature up to 500 °C, the diffraction patterns become narrower (reduction of $\beta$), which means that the average crystallite size increases to 41 nm.

FT-IR analysis of the $Ag_3PO_4$ powder yields two strong bands in the $1070-730$ $cm^{-1}$ and $580-445$ $cm^{-1}$ ranges, related to the vibrations of PO4 groups in its structure (figure not shown). The band at 940 $cm^{-1}$ with a small shoulder around 1055 $cm^{-1}$ is assigned to the P-O symmetric and asymmetric stretching mode, while the latter around 547 $cm^{-1}$ is related to O-P-O deformation [39].

ICP-AES analyses were performed to determine the chemical elements in the converted $Ag_3PO_4$ powder. Elemental analysis reveals the presence of phosphorus (P) and silver (Ag) with a molar ratio Ag/P = 2.98 (%Ag = 76.91, %P = 7.41), which is very close to the stoichiometric value of 3.0 for $Ag_3PO_4$. This result confirms the successful synthesis of silver phosphate using natural phosphate as the phosphorus source. Moreover, the absence of any detectable calcium in the analysis suggests that no residual precursor or calcium phosphate from the natural phosphate remains in the final product. This high chemical purity is further supported by the X-ray diffraction (XRD) patterns, which exclusively display the characteristic peaks of $Ag_3PO_4$, indicating the formation of a single, well-crystallized phase.

To elucidate the morphological properties of the prepared $Ag_3PO_4$ from natural phosphate, figure 5 shows the SEM images. In the lower magnification, the surface of the structured $Ag_3PO_4$ consists in a large amount of agglomerated particles having irregular spherical structures, while the higher magnification image in Fig. 5 (b) clearly reveals tetrahedron-like $Ag_3PO_4$ microcrystals.

The surface porosity of the powders was determined from $N_2$ sorption measurements using the BET and BJH methods (Fig. 6). Powders exhibit a type IV hysteresis loop, suggesting the presence of mesoporosity. The calculated specific surface area SBET of $Ag_3PO_4$ from BET was estimated to be ca. 50 $m^2/g$, higher than that of the NP mineral (20 $m^2/g$). The average pore size, $D_p$, was 7.4 nm for $Ag_3PO_4$ and slightly larger (10 nm) for NP. After heat treatment of silver phosphate at 500 °C, all $S_{BET}$ and $V_p$ values decreased slightly, to $S_{BET} = 38$ $m^2/g$ and $V_p = 0.12$ $cm^3/g$, and average pore size ($D_p$) to 5.1 nm, linked to grain growth

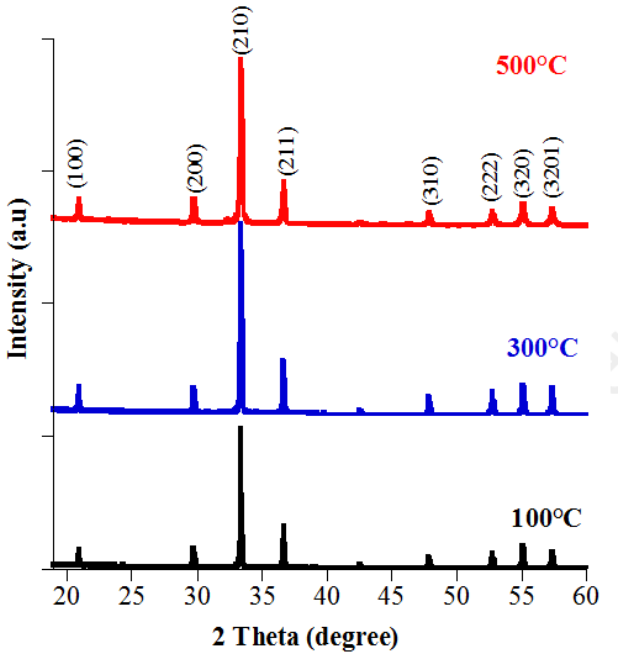


**Figure 4.** X-ray diffraction patterns of $Ag_3PO_4$ powder prepared and dried at 100 °C, then calcined at 300 °C and 500 °C.

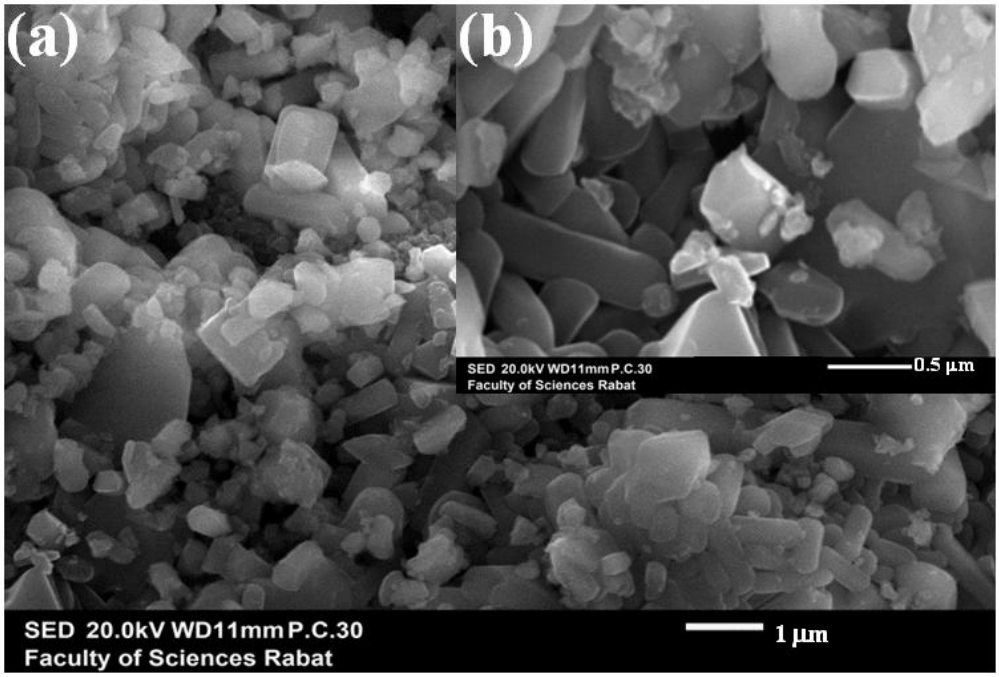


**Figure 5.** SEM images of calcined $Ag_3PO_4$ at 500 °C at two magnifications.

during calcination.

Diffuse reflection spectroscopy (DRS) was assessed to study the optical properties of the prepared powders (Fig. 7 (a)). $Ag_3PO_4$ shows a peak in the UV region ($< 400$ nm), proving its absorption in the visible. Its gap energy was estimated by the Wood-Tauc's equation [40]: $(\alpha h\nu)^{1/n} = A(h\nu - E_g)$, where $\alpha$ is the wavelength dependent absorption coefficient, $h$ is Planck constant, $E_g$ is the optical band gap of the semiconductor, $\nu$ is light frequency, $A$ is a proportionality constant, $n$ is Tauc exponent. $E_g$ is determined by extrapolating the linear portion of the $(\alpha h\nu)^2$ plots against $h\nu$ to the energy axis (Fig. 7 (b)). The $E_g$ value of the dried sample is calculated to be about 2.47 eV, which agrees with the literature [31, 41].

### 3.3 Photodegradation tests

The kinetic degradation of the three OTC concentrations (5, 10, 20 mg/L) was studied in the presence of 2 g/L of $Ag_3PO_4$ powder under visible light (Fig. 8). A preliminary adsorption period of 30 min was run in the dark before exposure to visible light. In the absence of the catalyst (photolysis), there is no reduction in the initial concentration of OTC over time, suggesting the absence of photochemical reactions. As shown in figure 8, a significant degradation of OTC was achieved in the presence of the photocatalyst, which is more significant for low OTC concentrations. In the dark, the decrease in the OTC concentration can only be explained by its adsorption onto the porous $Ag_3PO_4$ surface. This step is essential for the fixation of OTC molecules onto the $Ag_3PO_4$ catalyst, to permit further degradation under visible light. In the presence of both catalysts and

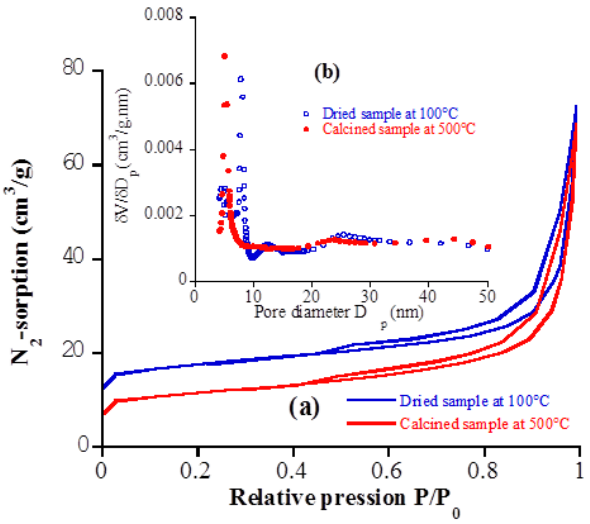


**Figure 6.** (a) $N_2$ sorption isotherms and (b) pore distribution on the surface of $Ag_3PO_4$ dried and calcined at 500 °C.

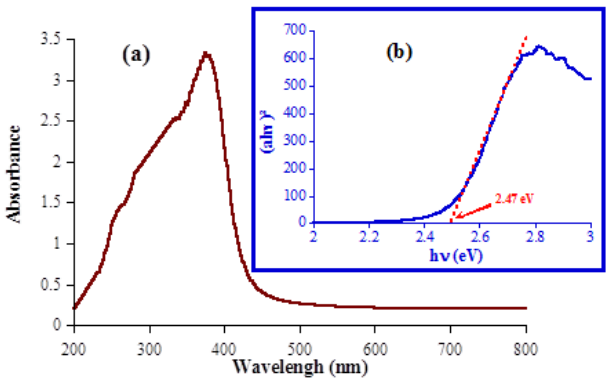


**Figure 7.** (a) UV-Vis absorbance spectrum and (b) plot $(\alpha h\nu)^2$ vs $h\nu$ for $Ag_3PO_4$ powder.

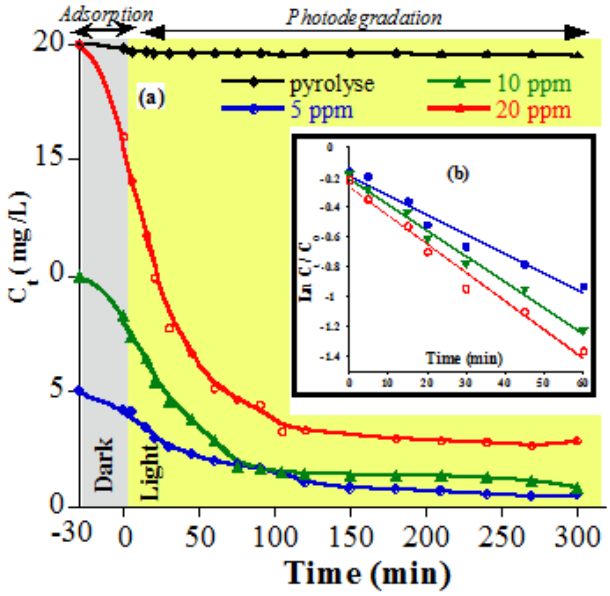


**Figure 8.** (a) Kinetics of degradation efficiency of the converted $Ag_3PO_4$ photocatalyst under visible light at different initial OTC concentrations, and (b) the Langmuir-Hinshelwood mechanism ($\ln(C_0/C_t)$ vs. time).

light, significant degradation of the antibiotic is observed. Higher concentration lengthens the time required for effective degradation. This change in catalytic performance is explained by saturation of the surface by OTC molecules, followed by masking the visible light, lowering radical generation, and consequently decreasing photocatalytic activity. The degradation kinetics generally depend on the characteristics of the catalyst, such as its structure and porosity, as well as on the concentration of the pollutant. This process obeys the pseudo-first order model, derived from the Langmuir-Hinshelwood equation [43, 44]: $\ln(C_t/C_0) = k_{app} \cdot t$, where $k_{app}$ is the apparent rate constant ($min^{-1}$), $C_0$ and $C_t$ are the initial and the instantaneous concentration of OTC (mg/L), $t$ is the irradiation time (min). The calculation of $k_{app}$ was restricted to the portion of the curve showing significant degradation, excluding the initial adsorption phase and any potential saturation effects. A strong linear relationship was observed between $\ln(C_t/C_0)$ versus irradiation time ($t$), with correlation coefficients ($R^2$) ranging from 0.98 to 0.99, confirming that the degradation process follows a pseudo-first-order kinetic model (Fig. 8 (b)). The apparent rate constant kapp increases with rising OTC concentrations, with values of 0.013 $min^{-1}$, 0.017 $min^{-1}$, and 0.018 $min^{-1}$ for 5, 10, and 20 mg/L, respectively. This trend reflects the greater availability of OTC molecules interacting with the catalyst surface, enhancing the degradation efficiency. At low pollutant concentration, photons can easily reach the catalyst surface, promoting radical formation, where OTC degradation is inversely proportional to the initial pollutant concentration. Although heat treatment of the $Ag_3PO_4$ did not affect its crystalline phase, it nevertheless reduced its porosity, and in turn affected the retention of the pollutant on the surface of the photocatalyst before its degradation under visible light.

Figure 9 (a) highlights the evolution of the photodegradation efficiency of the $Ag_3PO_4$ powder as a function of treatment temperatures. After a period of 30 minutes in the dark, it is observed that the retention rate of the antibiotic gradually decreases with increasing calcination temperature, where the OTC removal was 92%, 87%, and 84% at 100 °C, 300 °C, and 500 °C, respectively. This reduction is directly linked to the reduction in the porosity of the material, highlighting the importance of the porosity parameter in the interaction between $Ag_3PO_4$ and OTC molecules. As the $Ag_3PO_4$ structure is unaffected by the temperature of calcination, the specific surface area is an important parameter affecting the catalytic activity. A good linear correlation was observed between $\ln(C_0/C_t)$ and irradiation time ($t$), with correlation coefficients ($R^2$) ranging from 0.97 to 0.99, confirming that the degradation process follows first-order kinetics, and was found to be 0.034, 0.030, and 0.018 $min^{-1}$ for $Ag_3PO_4$ thermally treated at 100 °C, 300 °C, and 500 °C, respectively (Fig. 9 (b)). These results demonstrate that thermal treatment significantly influences the photocatalytic performance, with lower temperatures favoring higher degradation rates. Although $Ag_3PO_4$ calcined at 500 °C displays slightly lower photocatalytic performance compared to samples treated at 100 °C and 300 °C, this calcination temperature offers a notable advantage for catalyst reuse across multiple photocatalytic cycles. In particular, it promotes the thermal decomposition of residual pollutants and by-products, thereby contributing to improved catalyst regeneration and long-term operational stability.

The pH of the aqueous OTC solution is also an essential variable in photocatalysis applied to wastewater treatment. The reason is that it influences the surface charge and the size of the photocatalyst aggregates, and therefore, the elimination of pollutants from water. Figure 10 shows that the catalytic efficiency increases when the pH decreases. The maximum degradation of OTC is observed at pH 4, with a degradation rate of 87%. The best photocatalytic performances of $Ag_3PO_4$ are observed under acidic pH between pH 4 and 6, which is compatible with the pH of most waters.

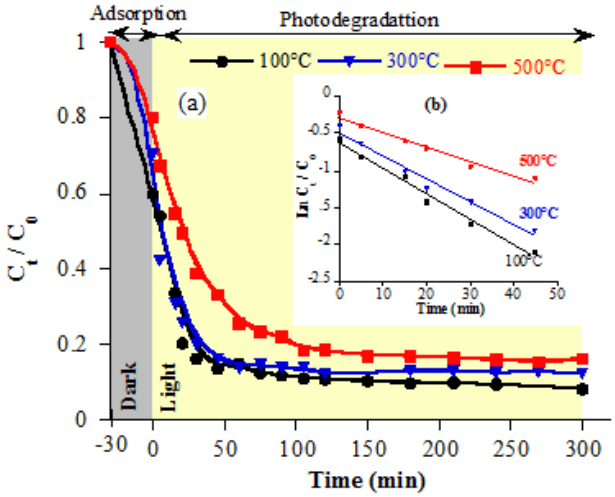


**Figure 9.** (a) Photocatalytic efficiencies of $Ag_3PO_4$ dried at 100 °C and calcined at 300 °C and 500 °C vs. OTC degradation ($C_0$ = 20 mg/L. dose = 2 g/L, pH 4), and (b) the Langmuir-Hinshelwood mechanism ($\ln(C_0/C_t)$ vs. time).

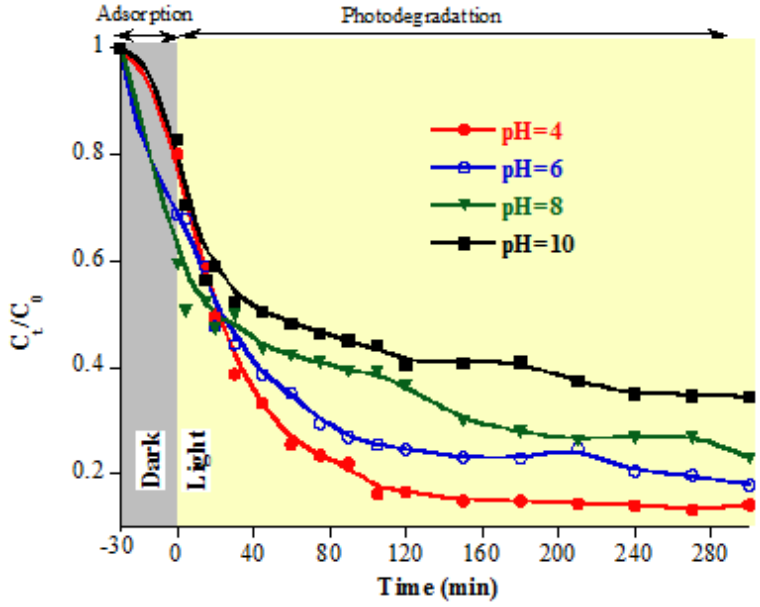


**Figure 10.** Effect of pH on the photodegradation of OTC supported on converted $Ag_3PO_4$.

This is thanks to the electrostatic attraction between the protonated surface of $Ag_3PO_4$ and the antibiotic. Indeed, surface protonation in an acidic environment also promotes the formation of hydroxyl radicals ($^{\bullet}OH$) under visible light, improving photodegradation, as proven in the mineralization of several organic pollutants [3, 7, 17].

In aqueous solutions, the pH affects both the surface charge of the photocatalyst particles and possibly the nature of the species to be degraded, i.e., the state of the pollutant according to its $pK_a$. The pH at which the surface charge is zero (called $pH_{pzc}$) is an important characteristic for an adsorbent or a photoactive material; it is 6.8 for $Ag_3PO_4$ [39]. For different values of this pH, the photocatalyst surface is charged. If pH is higher than $pH_{pzc}$, the catalyst surface is negatively charged. If pH is lower than $pH_{pzc}$, it has a positive charge. The change in pH can affect the ionized pollutant and the surface charge of the catalyst, which affects the adsorption/desorption properties and consequently the photocatalytic efficiency [43–46]. Oxytetracycline has three $pK_a$ values: $pK_{a1}$ at 3.2 (Enolic and carboxamide), $pK_{a1}$ = 7.4 (Diketopenolic), and $pK_{a1}$ = 8.9 (Ethyamine) [42]. In aqueous or polar media, OTC manifests an amphoteric character with an isoelectric point at pH 5. The structure and pH-dependent surface speciation of OTC antibiotic in aqueous solutions are illustrated in figure 11, showing the three ionic forms (cationic, anionic, and neutral).

At pH 4 – 6, the neutral species of OTC are predominant and favorably adsorbed on the surface of $Ag_3PO_4$ followed by rapid photodegradation. Under basic conditions (pH 8 and 10), there are more hydroxyl ions present on the $Ag_3PO_4$ surface, which interact with the negative OTC form, causing repulsion and disfavoring the adsorption. This justifies the decrease in the apparent initial degradation constant of OTC. Therefore, the degradation of OTC molecules is strongly linked to the ionization states of the catalyst and substrate surface during photocatalysis.

Material stability and reusability are important parameters that reduce processing costs. As a cycle, the powder was regenerated by washing with distilled water, dried at 100 °C, calcined at 500 °C, and then reused for the next cycle. The performance of $Ag_3PO_4$ decreased slightly after each cycle, from 86% (first cycle) to 78.5% (fifth cycle). XRD patterns permit understanding the photo-stability of $Ag_3PO_4$. XRD clearly confirms the presence of the initial $Ag_3PO_4$ phase

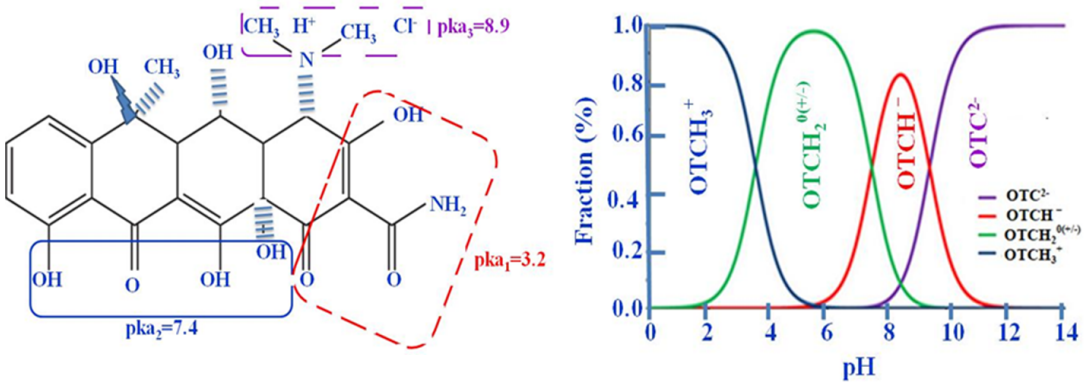


**Figure 11.** Structure and pH-dependent surface speciation of oxytétracycline [42].

and shows that photocorrosion of $Ag_3PO_4$ can take place, thereby limiting their practical applications. To avoid this, the $Ag_3PO_4$ surface should be decorated with inhibitors to block the subsequent $Ag^+ \rightarrow Ag^0$ reduction, as described in earlier research [47–49].

To describe the photocatalytic mechanism of $Ag_3PO_4$ under visible light, a mechanism based on the respective positions of the conduction (CB) and valence (VB) bands of $Ag_3PO_4$ is considered. The conduction (BC) and valence (BV) band edge potentials for $Ag_3PO_4$ are +0.45 eV and +2.9 eV, respectively. Under visible light, electrons in the VB are excited towards the CB, leaving separate holes ($h^+$) in the VB, which are the most important reactive oxidative species affecting the photocatalytic efficiency and oxidizing the OTC molecules directly [50, 51]. Since the VB potential of $Ag_3PO_4$ (+2.47 eV) is positive and close to $E_g$ ($^\bullet OH/H_2O$) (2.68 eV), holes could also react with $H_2O$ to produce $^\bullet OH$ radicals [52].

Note that the energy of the $Ag_3PO_4$ conduction band at 0.45 eV is higher than that of the standard hydrogen electrode ($E(O_2/^\bullet O_2^-) = -0.33$), which means that it cannot produce $^\bullet O_2^-$ from dioxide ($O_2$). Part of the conduction band electrons of $Ag_3PO_4$ can be efficiently transferred to the surface of metallic $Ag^0$ thanks to the Schottky barrier formed at the metal-to-semiconductor interface. Ag nanoparticles can then transfer the injected and accumulated electrons to $O_2$ to form $^\bullet O_2^-$ [52]. A possible photocatalytic mechanism for $Ag_3PO_4$ under visible light is proposed in figure 12. In fact, the produced electron can now be captured by oxygen, producing superoxide radicals ($^\bullet O_2^-$) on the surface, and by interacting with $OH^-$ ions, holes in the VB generate hydroxyl radicals ($^\bullet OH$). These $^\bullet O_2^-$ and $^\bullet OH$ radicals can then attack the OTC molecules via a series of redox reactions, thereby degrading this antibiotic. The degradation process can be summarized by the following chemical reactions:

$$Ag_3PO_4 + h\nu \rightarrow {e_{CB}}^- + {h_{VB}}^+ \quad \text{(Eq. 1)}$$

$${e_{CB}}^- + O_2 \rightarrow {}^\bullet O_2^- \quad \text{(Eq. 2)}$$

$${h_{VB}}^+ + OH^- \rightarrow {}^\bullet OH \quad \text{(Eq. 3)}$$

$$({}^\bullet OH, {}^\bullet O_2^-, {h_{VB}}^+) + OTC \rightarrow CO_2 + H_2O \quad \text{(Eq. 4)}$$

It is concluded that the low-cost mesoporous $Ag_3PO_4$ prepared from natural phosphate is a promising catalyst for the photocatalytic degradation of dyes from industrial wastewater. Although few works reported photodegradation of the OTC antibiotic on the $Ag_3PO_4$ compound, many reported the photodegradation of other organic pollutants on its composites. Our results show that the low-cost $Ag_3PO_4$ converted from natural phosphate is an efficient photocatalyst under LED-visible light, in comparison with most silver-based phosphate photocatalysts described in the literature [49, 53, 54]. This implies that $Ag_3PO_4$ can be a suitable photocatalyst for drug degradation in wastewater. Its efficiency should be improved by combination with conductive oxides such as graphene oxide (GO) and tricyanomethanide g-$C_4N_3$.

## 4. Conclusion

This study demonstrates the feasibility of the preparation of $Ag_3PO_4$ from natural phosphate and its effective use as a photocatalyst for the degradation of the OTC antibiotic loaded with harmful organic residues. The prepared materials were carefully characterized, confirming the formation of the pure mesoporous $Ag_3PO_4$ phase. Formation of this pure phase is affected by the pH of the reaction. Photodegradation of OTC antibiotic on dried calcined catalysts under visible light was achieved. In the simultaneous presence of the photoactive $Ag_3PO_4$ and visible light, degradation of the antibiotic depends on the preparation of the photocatalyst and the pH of the contaminated solution. The $Ag_3PO_4$ particles activate this catalysis by absorbing the visible light to give rise to very reactive $^\bullet OH$ radical species, which lead to the degradation

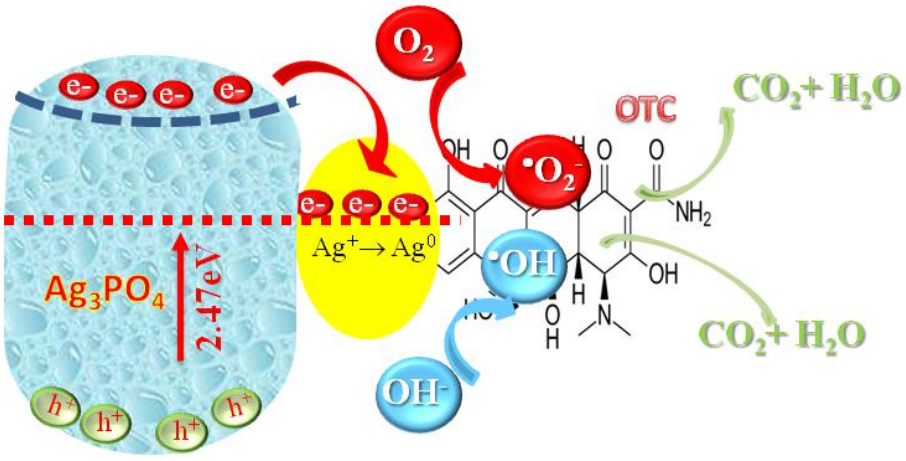


**Figure 12.** Illustration of the photocatalytic degradation of OTC on the $Ag_3PO_4$ catalyst.

of the organic matter contained in the solution.

**Acknowledgements**
This research was supported by Mohammed V University (Morocco) and Queen's University (Natural Sciences and Engineering Research Council of Canada NSERC, RGPIN-2020-07016).

**Authors contributions**
Authors have contributed equally in preparing and writing the manuscript.

**Availability of data and materials**
The data that support the findings of this study are available from the corresponding author, upon reasonable request.

**Conflict of interests**
The author declare that they have no known competing financial interests or personal relationships that could have appeared to influence the work reported in this paper.

## References

[1] K. Sun, Q. Lyu, X. Zheng, R. Liu, C. Y. Tang, M. Zhao, and Y. Dong. *Water Res.*, **254**(2024):121395. DOI: https://doi.org/10.1016/j.watres.2024.121395.

[2] S. Laasri A. Laghzizil A. Saoiabi C. El Bekkali, H. Bouyarmane. *Iranian J. Catal.*, **8**(2018):241–247. URL https://oiccpress.com/ijc/article/view/4015.

[3] C. Ting, C. Chen, Y. Chenhao, X. Weifang, Z. Xiao, and T. Yuan. *Iran. J. Chem. Chem. Eng.*, **41**(2022):1942–1960.

[4] C. El Bekkali, M. Abbadi, J. Labrag, I. Es-saidi, D. Robert, J. M. Nunzi, and A. Laghzizil. *Chemistry Africa*, **7**(2024):3883–3892, . DOI: https://doi.org/10.1007/s42250-024-00982-7.

[5] A. Yousefi and A. Nezamzadeh-Ejhieh. *Iran. J. Catal.*, **11**(2021): 247–259. URL https://oiccpress.com/ijc/article/view/3600.

[6] C. El Bekkali, H. Bouyarmane, M. El Karbane, S. Masse, A. Saoiabi, T. Coradin, and A. Laghzizil. *Colloid Surf. A*, **539**(2018):364–370, . DOI: https://doi.org/10.1016/j.colsurfa.2017.12.051.

[7] S. Leong, A. Razmjou, K. Wang, K. Hapgood, X. Zhang, and H. Wang. *J. Membrane Sci.*, **472**(2014):167–184. DOI: https://doi.org/10.1016/j.memsci.2014.08.016.

[8] M. Li, N. H. Shah, P. Zhang, P. Chen, Y. Cui, Y. Jiang, and Y. Wang. *Mater. Today Sustain.*, **22**(2023):100409, . DOI: https://doi.org/10.1016/j.mtsust.2023.100409.

[9] S. Jafari and A. Nezamzadeh-Ejhieh. *J. Colloid Interf. Sci.*, **490**(2017):478–487. DOI: https://doi.org/10.1016/j.jcis.2016.11.087.

[10] H. Derikvandi, M. Vosough, and A. Nezamzadeh-Ejhieh. *Inter. J. Hydrogen Energy*, **46**(2021):2049–2064. DOI: https://doi.org/10.1016/j.ijhydene.2020.10.065.

[11] M. Karimi-Shamsabadi and A. Nezamzadeh-Ejhieh. *J. Mol. Catal. A: Chemical*, **418-419**(2016):103–114. DOI: https://doi.org/10.1016/j.molcata.2016.03.034.

[12] S. El-Hout, S. M. Abdou, and S. M. El-Sheikh. *Inter. J. Mater. Technol. Innovation*, **4**(2024):32–41. DOI: https://doi.org/10.21608/ijmti.2024.291301.1104.

[13] G. Botelho, J. Andres, L. Gracia, L. S. Matos, and E. Longo. *ChemPlusChem.*, **81**(2016):202– 212. DOI: https://doi.org/10.1002/cplu.201500485.

[14] M. Rezaei, A. Nezamzadeh-Ejhieh, and A. R. Massah. *Mater. Today Energy*, **48**(2025):101754, . DOI: https://doi.org/10.1016/j.mtener.2024.101754.

[15] T. A. Vu, C. D. Dao, T. T. T. Hoang, K. T. Nguyen, G. H. Le, P. T. Dang, H. T. K. Tran, and T. V. Nguyen. *Mater. Letters*, **92**(2013): 57–60. DOI: https://doi.org/10.1016/j.matlet.2012.10.023.

[16] H. Katsumata, M. Taniguchi, S. Kaneco, and T. Suzuki. *Catalysis Comm.*, **34**(2013):30–34. DOI: https://doi.org/10.1016/j.catcom.2013.01.012.

[17] C. Yu, X. Chen, N. Li, et al. *Environ. Sci. Pollut. Res.*, **29**(2022): 18423–18439. DOI: https://doi.org/10.1007/s11356-022-18591-7.

[18] A. Amirulsyafiee, M. M. Khan, M. Y. Khan, A. Khan, and M. H. Harunsani. *Solid State Sci.*, **131**(2022):106950. DOI: https://doi.org/10.1016/j.solidstatesciences.2022.106950.

[19] K. Danoun, R. Tabit, A. Laghzizil, and M. Zahouily. *BMC Chem.*, **15**(2021):42. DOI: https://doi.org/10.1186/s13065-021-00767-w.

[20] F. Teng, Z. Liu, and A. Zhang. *Environ. Sci. Technol.*, **49**(2015): 9489. DOI: https://doi.org/10.1021/acs. est.5b00735.

[21] J. Luo, Y. Luo, Q. Li, J. Yao, G. Duan, and X. Liu. *Colloid. Surf. A*, **535**(2017):89–95. DOI: https://doi.org/10.1016/j.colsurfa.2017.09.032.

[22] S. Uyi, Sulaeman, Gandasasmita, Y. Diastuti, H. Iswanto, P. Isnaeni, T. Ardiansyah, and Y. Shu. *Surf. Interf.*, **28**(2022):101672. DOI: https://doi.org/10.1016/j.surfin.2021.101672.

[23] K. Afifah, R. Andreas, D. Hermawan, and U. Sulaeman. *Bull. Chem. React. Eng. Catal.*, **14**(2019):625. DOI: https://doi.org/10.9767/bcrec.14.3.4649.625- 633.b.

[24] Y. Bi, H. Hu, S. Ouyang, G. Lu, J. Cao, and J. Ye. *Chem. Commun.*, **48**(2012):3748. DOI: https://doi.org/10.1039/c2cc30363a.

[25] J. Deng, H. Pang, D. Deng, and J. Zhang. *Proc. Inst. Mech. Eng. Part N J. Nanoeng. Nanosyst.*, **225**(2011):67–69. DOI: https://doi.org/10.1177/ 1740349912436450.

[26] X. Song, R. Li, M. Xiang, S. Hong, K. Yao, and Y. Huang. *Ceram. Inter.*, **43**(2017):4692–4701. DOI: https://doi.org/10.1016/j.ceramint.2016.12.124.

[27] X. Guan, J. Shi, and L. Guo. *Inter. J. Hydrogen Energy*, **38**(2013): 11870–11877. DOI: https://doi.org/10.1016/j.ijhydene.2013.07.017.

[28] J. F. Cruz-Filho, T. M. S. Costa, M. S. Lima, L. J. Silva, R. S. Santos, L. S. Cavalcante, E. Longo, and G. E. Luz. *J. Photochem. Photobiol. A Chem.*, **377**(2019):14–25. DOI: https://doi.org/10.1016/j.jphotochem.2019.03.031.

[29] Y. Liu, L. Fang, H. Lu, Y. Li, C. Hu, and H. Yu. *Appl. Catal. B Environ.*, **115-116**(2012):245–252. DOI: https://doi.org/10.1016/j.apcatb.2011.12.038.

[30] J. Balachandramohan, R. Singh, T. Sivasankar, and S. Manickam. *Chem. Eng. Proces.- Process Inten.*, **168**(2021):108549. DOI: https://doi.org/10.1016/j.cep.2021.108549.

[31] H. El Masaoudi, I. Benabdallah, B. Jaber, A. Laghzizil, and M. Benaissa. *J. Nanostruct.*, **10**(2021):362–374. DOI: https://doi.org/10.22052/JNS.2020.02.015.

[32] G. He, W. Yang, W. Zheng, L. Gong, X. Wang, Y. An, and M. Tian. *RSC Adv.*, **9**(2019):18222–18231. DOI: https://doi.org/10.1039/c9ra01306g.

[33] S. El Asri, A. Laghzizil, T. Coradin, A. Saoiabi, A. Alaoui, and R. M'hamedi. *Colloid. Surf. A*, **362**(2010):33–38.
DOI: https://doi.org/10.1016/j.colsurfa.2010.03.036.

[34] S. Saoiabi, S. El Asri, A. Laghzizil, A. Saoiabi, J. L. Ackerman, and T. Coradin. *Chem. Eng. J.*, **211-212**(2012):233–239.
DOI: https://doi.org/10.1016/j.cej.2012.09.017.

[35] H. Bouyarmane, C. El Bekkali, J. Labrag, I. Es-saidi, O. Bouhnik, H. Abdelmoumen, A. Laghzizil, J. M. Nunzi, and D. Robert. *Surf. Interf.*, **24**(2021):101155.
DOI: https://doi.org/10.1016/j.surfin.2021.101155.

[36] K. Fanidi, K. Bouiahya, A. Gouza, A. Saoiabi, and A. Laghzizil. *Desal. Water Treat.*, **100**(2017):145–150.
DOI: https://doi.org/10.5004/dwt.2017.21803.

[37] I. Es-saidi, J. Labrag, A. Laghzizil, and J.-M. Nunzi. *Solid State Sci.*, **111**(2021):106440.
DOI: https://doi.org/10.1016/j.solidstatesciences.2020.106440.

[38] S. Sharafzadeh, J. Zolgharnein, A. Nezamzadeh-Ejhieh, and S. Dermanaki Farahani. *Surf. Interf.*, **59**(2025):105917, .
DOI: https://doi.org/10.1016/j.surfin.2025.105917.

[39] N. Raeisi-Kheirabadi and A. Nezamzadeh-Ejhieh. *Inter. J. Hydrogen Energy*, **45**(2020):33381–33395.
DOI: https://doi.org/10.1016/j.ijhydene.2020.09.028.

[40] M. Al Kausor, S. Sen Gupta, and D. Chakrabortty. *J. Saudi Chem. Soc.*, **24**(2020):20–41.
DOI: https://doi.org/10.1016/j.jscs.2019.09.001.

[41] M. Rezaei, A. Ensafi, and E. Heydari-Bafrooei. *J. Ind. En. Chem.*, (2024):228–240, .
DOI: https://doi.org/10.1016/j.jiec.2024.11.043.

[42] Y. Li, H. Wang, X. Liu, G. Zhao, and Y. Sun. *Environ. Sci. Poll. Res. Inter.*, **23**(2016):13822–31, .
DOI: https://doi.org/10.1007/s11356-016-6513-8.

[43] A. Nezamzadeh Ejhieh and M. Khorsandi. *J. Hazard. Mater.*, **176**(2010):629–637.
DOI: https://doi.org/10.1016/j.jhazmat.2009.11.077.

[44] M. Rezaei, A. Nezamzadeh-Ejhieh, and A. R. Massah. *Ecotoxicol. Environ. Saf.*, **269**(2024):115927, .
DOI: https://doi.org/10.1016/j.ecoenv.2024.115927.

[45] M. Rezaei, M. Nezamzadeh-Ejhieh, A. Massah, and A. Reza. *Energy Fuels*, **38**(2024):7637, .
DOI: https://doi.org/10.1021/acs.energyfuels.4c00325.

[46] M. Rezaei and A. Nezamzadeh-Ejhieh. *Inter. J. Hydrogen Energy*, **45**(2020):24749–24764.
DOI: https://doi.org/10.1016/j.ijhydene.2020.06.258.

[47] M. E. Taheri, A. Petala, Z. Frontistis, D. Mantzavinos, and D. I. Kondarides. *Catal. Today*, **280**(2017):99–107.
DOI: https://doi.org/10.1016/j.cattod.2016.05.047.

[48] A. Oulguidoum, S. Fatine, M. Abbadi, A. Bouziani, Z. Boujmlaoui, J. M. Nunzi, and A. Laghzizil. *Environ. Sci. Pollut. Res.*, **32**(2025):2267–2279.
DOI: https://doi.org/10.1007/s11356-024-35855-6.

[49] Q. Yan, C. Li, C. Lin, Y. Zhao, and M. H. Zhang. *J. Mater. Sci.-Mater.*, **29**(2018):2517–2524.
DOI: https://doi.org/10.1007/s10854-017-8174-x.

[50] C. Cui, Y. Wang, D. Liang, et al. *Appl. Catal. B Environ.*, **158**(2014):150–160.
DOI: https://doi.org/10.1016/j.apcatb.2014.04.007.

[51] S. Sharafzadeh, J. Zolgharnein, A. Nezamzadeh–Ejhieh, and S. Dermanaki Farahani. *Inter. J. Hydrogen Energy*, **106**(2025):1429–1442, .
DOI: https://doi.org/10.1016/j.ijhydene.2025.02.031.

[52] S. Ma, J. Xue, Y. Zhou, and Z. Zhang. *RSC Adv.*, **5**(2015):40000–6.
DOI: https://doi.org/10.1039/C5RA04075B.

[53] K. Ouyang, N. Jiang, W. Xue, and S. Xie. *Colloids and Surfaces A*, **604**(2020):125312.
DOI: https://doi.org/10.1016/j.colsurfa.2020.125312.

[54] F. Wu, F. Zhou, Z. Zhu, S. Zhan, and Q. He. *Chem. Phys. Lett.*, **724**(2019):90–95.
DOI: https://doi.org/10.1016/j.cplett.2019.03.058.